Clays and Clay Minerals, Vol. 57, No. 6, 751–770, 2009.

RAPID DEHYDROXYLATION OF NICKELIFEROUS GOETHITE IN LATERITIC NICKEL ORE: X-RAY DIFFRACTION AND TEM INVESTIGATION

MATTHEW LANDERS[1,*], ROBERT J. GILKES[1], AND MARTIN A. WELLS[2]

[1] School of Earth and Environment (M087), University of Western Australia, 35 Stirling Highway, Crawley, WA 6009, Australia
[2] CSIRO, Exploration and Mining, Australian Resource Research Centre (ARRC), PO Box 1130, Bentley, WA 6102, Australia

Abstract—A method for extracting Ni and other metals from lateritic ores by means of shock heating has been investigated. Shock heating releases some of the metal from its goethitic host. Even though the transformation of pure goethite to hematite is known to occur *via* intermediate hydroxylated phases, the effect of other metals such as Ni substituting for Fe in goethites on this thermal transformation to hematite is unknown. The purpose of this study was to fill this gap, with the hope that the results will lead to more energy-efficient extraction methods and/or a better understanding of Fe geochemistry in thermally activated soils. X-ray diffraction, transmission electron microscopy with EDS, and thermal analysis were used to investigate mineralogical changes in nickeliferous goethites from five oxide-type lateritic nickel ore deposits that had been subjected to shock heating at temperatures in the range 220−800ºC. Acicular, nano-sized goethite was the main constituent of the samples with minor to trace amounts of quartz, talc, kaolinite, chromite, maghemite, and Mn oxides. Goethite was partially dehydroxylated to OH-hematite at 340−400ºC and had completely altered to well ordered hematite at 800ºC. The OH-hematite was characterized by broad XRD peaks for reflections associated with the Fe sublattice. The goethite unit-cell *a* and *b* lengths remained almost constant with increasing preheating temperature up to 300ºC, while the size of the *c* axis dimension contracted. The neoformed hematite crystals were larger than the precursor goethite crystals due to development, by sintering and surface diffusion, of regularly ordered hematite domains. The increase (1.5−2.6 fold) in surface area with increasing heating temperature (up to 340−400ºC) reflected the development of slit-shaped micropores (~300ºC), which further developed into elliptically shaped micropores (~400ºC) in OH-hematite. With increased heating temperature, well ordered hematite formed with only a few micropores remaining. Such results may contribute to the development of more efficient procedures for extracting Ni from lateritic nickel ores, as the rate of dissolution of goethite in acid in 'heap and pressure' leach facilities will be enhanced by the increases in surface area and microporosity. The results may also provide valuable information on the probable effects of natural heating on pedogenic Fe oxides.

Key Words—Dehydroxylation, Goethite, Lateritic, Ni Ore, Shock Heating, TEM, XRD.

INTRODUCTION

Oxide-type (limonitic) nickeliferous laterites occur as a result of weathering of ultramafic rocks containing olivine, pyroxene, and amphibole, which have Ni contents between 0.2 and 0.4% (Golightly, 1981). Divalent Fe is oxidized and precipitates from soil solution as microcrystalline ferric (oxyhydr)oxides (predominantly goethite [α-FeOOH] with lesser hematite [α-Fe_2O_3]), and Ni is concentrated in the goethite at 3−30 times the concentration of the parent rock.

Isomorphous substitution of Al^{3+} for Fe^{3+} within the structure of natural goethite commonly occurs and has been investigated widely, as have synthetic Al-substituted goethites. A number of other metals can replace Fe in synthetic goethite and hematite: these include Cr (Schwertmann *et al*., 1989), Mn (Stiers and Schwertmann, 1985; Alvarez *et al*., 2007), Ge (Bernstein and Waychunas, 1987), V (Schwertmann and Pfab, 1996), Co (Pozas *et al.*, 2004), Ni, Cu, Zn, Cd, and Pb (Gerth, 1990), and Ti (Wells *et al*., 2006). The properties (*e.g.* valence state, ionic radius) of the substituted metals variously affect the properties of the Fe oxides (*e.g.* unit-cell dimensions, crystal size, and crystallinity).

Goethite dehydroxylates topotactically to hematite on heating, and this process has been the focus of numerous studies due to *inter alia*: (1) the wide technological applications of Fe oxides (*e.g.* magnetic recording devices); (2) the thermal transformation is the basis of some mineral processing techniques (*e.g.* iron ore industry); (3) dehydroxylation occurs in nature due to natural and managed forest and grassland fires (Anand and Gilkes, 1987), and is, therefore, of interest to soil scientists (Wolska and Schwertmann, 1989; Singh and Gilkes 1992a); and (4) the thermal transformation has been studied by archaeologists because the Fe oxide pigments, goethite (yellow) and hematite (red), were used by pre-historic artists who apparently created red pigments by heating goethite (Pomiès *et al*., 1999; Frost *et al*., 2003; de Faria and Lopes, 2007). The present

* E-mail address of corresponding author:
10031821@student.uwa.edu.au
DOI: 10.1346/CCMN.2009.0570608

https://doi.org/10.1346/CCMN.2009.0570608 Published online by Cambridge University Press

study relates to the transformation of goethite for its potential application to improve the efficiency of Ni extraction from goethitic lateritic nickel ores by the 'heap leaching' process (Landers *et al*., 2008).

Conventional and synchrotron based X-ray diffraction (XRD), infrared (IR), and Raman spectroscopy have shown that dehydroxylation of goethite to well ordered hematite may involve the formation of intermediate metastable hematite-like phases, which contain residual hydroxyl units. Such partially dehydroxylated phases have been named protohematite and hydrohematite (Wolska, 1988; Wolska and Schwertmann, 1989; Gualtieri and Venturelli, 1999; Ruan *et al*., 2002; Wells *et al*., 2006). The first intermediate hematite-like phase (250–400ºC), known as protohematite, contains excess hydroxyl units and is Fe-deficient in comparison to well ordered (stoichiometric) hematite (Wolska and Schwertmann, 1989). The excess or non-stoichiometric OH^- mostly affects the unit-cell *a* dimension (Ruan and Gilkes, 1995). Gualtieri and Venturelli (1999) also observed the non-stoichiometric (*i.e.* Fe-deficient) composition of protohematite. The second intermediate hematite-like phase hydrohematite was identified by Wolska and Schwertmann (1989) and forms on heating above 430ºC and may be distinguished from hematite by the presence of IR bands at ~3400, 940–950, and 630 cm^{-1} (Wolska, 1988). At temperatures above 800ºC, hydrohematite transforms to well ordered hematite, which is characterized by the complete loss of residual OH and the achievement of hematite stoichiometry. Protohematite and hydrohematite have not yet been accepted as discrete mineral species, so for the remainder of this paper they will both be referred to collectively as OH-hematite. The studies cited above are based mostly on investigations of pure or unsubstituted goethite. The behavior of metals such as Ni within the structure of goethite during transformation to hematite is poorly understood. Some metals affect the dehydroxylation temperature of goethite and the properties of the resultant hematite (*e.g.* Al, Frost *et al*., 2003), due to the differences in strength of metal–OH bonds. Ni and other metals that are not compatible with the neoformed hematite structure are postulated to be exsolved and either reside on the crystal surface, in voids, or occur as inclusions of discrete phases (*e.g.* NiO) (Landers *et al*., 2008).

The purpose of the present research was to investigate the properties of five goethites from oxide-type lateritic Ni ores subjected to shock heating at various temperatures (220–800ºC). The structural and morphological changes associated with the transformation of goethite to hematite were investigated using XRD, thermal gravimetric/differential thermal analysis (TG/DTA), differential scanning calorimetry (DSC), and transmission electron microscopy (TEM) with energy dispersive spectrometry (EDS). Results from this research may contribute to the development of new and more energy-efficient procedures for processing oxide-type lateritic Ni ores. The results may also provide valuable information on the geochemistry of Fe oxides in soils as influenced by natural phenomena such as bush fires.

MATERIALS AND METHODS

Thirty-three oxide-type lateritic Ni samples were obtained from five deposits (Kalgoorlie and Ravensthorpe in Australia; Goro and Koniambo in New Caledonia; and Weda Bay in Indonesia). X-ray diffraction patterns of randomly oriented powders were obtained and the relative proportions of goethite and hematite were measured from the integrated intensities of the goethite 110 and hematite 102 reflections, respectively. For heterogeneous samples (*i.e.* diverse particle size and/or color), the different materials were handpicked from the samples for separate investigation by XRD (*e.g.* Ravensthorpe material). Where rock samples were too hard to grind by hand in an agate mortar and pestle, sub-samples were ground in a Saylon vessel in a Tema mill until all the material passed through a 75 μm mesh nylon sieve. From XRD analysis the most goethite-rich sample from each deposit was selected for further investigation (Figure 1).

Approximately 4 g sub-samples of each oven-dried (105ºC) goethite were weighed and then heated in air at 220, 240, 260, 280, 300, 320, 340, 400, 600, and 800ºC for 30 min in a laboratory furnace. Goethite was heated rapidly as a shallow layer (~1 mm thick) to minimize temperature gradients within the sample. Heating was on a ceramic plate that had previously been heated at 400ºC to remove any adsorbed water, and then cooled to air temperature. Samples were placed in a furnace that had been preheated to the desired temperature, to simulate the effect of an intense fire at the soil surface or rapid heating in an industrial autoclave (*i.e.* thermal shock). After 30 min samples were removed from the furnace and left to cool at 105ºC to prevent re-adsorption of moisture, and then weighed to enable calculation of the percentage loss of weight on heating (LOI). X-ray diffraction patterns were obtained for the heated samples. Chemical analysis of the bulk goethite samples was after dissolution in 2 M H_2SO_4 because this is the acid used in lateritic Ni refineries. The solutions were analysed using inductively coupled plasma mass spectrometry (ICP-MS). Analysis by X-ray fluorescence (XRF) was also conducted on the samples and the results were very similar to those obtained using 2 M H_2SO_4; only chemical analysis after dissolution in 2 M H_2SO_4 is, therefore, shown. If any residue was present after dissolution, XRD patterns were obtained to determine the insoluble phases.

The specific surface area for original and heated goethite was measured using a Micromeritics Gemini 2375 instrument with a VacPrep 061 and the 5 point BET method with N_2 as the adsorbate (Brunauer *et al.*,

https://doi.org/10.1346/CCMN.2009.0570608 Published online by Cambridge University Press

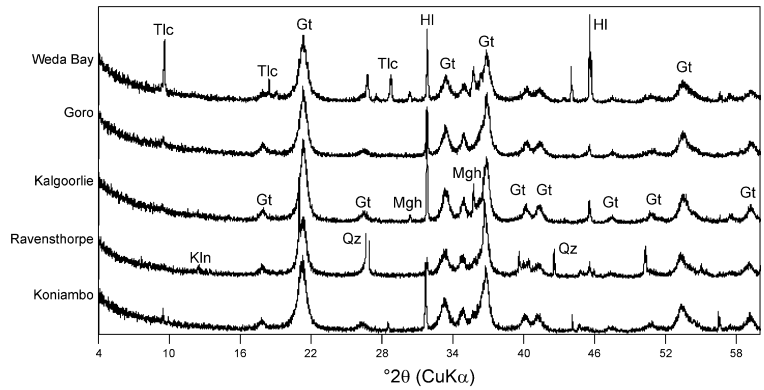

Figure 1. XRD patterns of five goethites from lateritic nickel deposits dried at 105ºC, with ~10% NaCl added as an internal standard. Appreciable amounts of impurity are present in some samples. Gt = goethite, Qz = quartz, Tlc = talc, Kln = kaolinite, Hl = halite, and Mgh = maghemite.

1938). The samples were pre-treated before the surface-area determination by degassing in a vacuum overnight at 105ºC.

X-ray diffraction patterns were obtained using a Philips PW 1830 X-ray diffractometer with a Cu target tube and a diffracted beam graphite monochromator. The XRD patterns were collected over the range 4–60º2θ at a scan rate of 0.3º2θ min^{-1} in 0.01º2θ steps. Approximately 10% by weight of halite (NaCl) was mixed with the sample to provide an internal standard for spacing and line-broadening measurements. After smoothing the patterns and correcting for displacement and background, the area and full width at half maximum intensity (FWHM) of the peaks were calculated using the *XPAS* program (Singh and Gilkes, 1992b). The mean crystal length (MCL) was calculated from FWHM values using the Scherrer equation (Klug and Alexander, 1974), with a K constant of 0.9. The FWHM and MCL were determined for the goethite (020), (110), (111), and (151) reflections, and for the hematite (110), (104), (012), (113), (024), and (116) reflections. Unit-cell dimensions and unit-cell volume were calculated using the online program *XLAT* (Rupp, 1988), from corrected positions of the goethite (020), (110), (120), (130), (021), (111), (121), (140), (211), (221), and (151) reflections, and from the hematite (012), (104), (110), (113), (024), and (116) reflections.

Simultaneous differential thermal analysis (DTA) and thermal gravimetric analysis (TGA) was conducted using a Perkin Elmer STA 6000 thermal analyser with *Pyris* software. Initially, different atmospheres (*i.e.* air and N_2) and sample weights (*i.e.* 10 mg and 50 mg) were evaluated using the Koniambo goethite to test if these factors affected thermal data, but no significant differences were observed. Approximately 10 mg goethite samples were heated from ambient temperature at a rate of 10ºC/min and dried isothermally at 105ºC for 10 min to a constant weight, and then heated to 1000ºC at a rate of 10ºC/min with the furnace purged using air flowing at 30 mL/min.

Transmission electron microscopy was used to investigate the morphology of the nanometric sized crystals for all unheated and heated goethites (*i.e.* goethite, OH-hematite, and hematite). Specimens were prepared by ultrasonically dispersing the sample in Milli-Q water and then placing a drop of the very dilute suspension onto a carbon-coated copper grid and air dried before examination. The TEM studies were performed on a JEOL 3000 FEG electron microscope operated at 300 kV with an image resolution of 0.14 nm. The TEM was equipped with a Gatan digital camera with 1024 × 1024 pixels, and an Oxford Instruments INCA 200 energy dispersive spectrometer (EDS). A JEOL 2100 TEM operated at 120 kV was used for selected area

Table 1. Chemical composition of the goethites (105ºC) based on dissolution in 2 M H_2SO_4.

	Fe (mg/g)	Al (mg/g)	Mn (mg/g)	Mg (mg/g)	Ti (mg/g)	Ni (mg/kg)	Cr (mg/kg)	V (mg/kg)	Cu (mg/kg)	Zn (mg/kg)	Co (mg/kg)	Gt content[a]
Weda Bay	429.20	20.60	5.50	2.50	2.50	9800	12600	200	90	220	870	79
Goro	440.50	13.40	43.90	1.60	1.80	5900	13600	130	130	330	1900	78
Kalgoorlie	446.70	7.80	13.00	3.90	2.60	8800	11300	60	70	400	1400	78
Ravensthorpe	392.40	0.90	2.50	3.20	0.30	12900	800	30	60	30	480	63
Koniambo	550.10	16.20	3.80	1.90	0.10	10200	13100	200	90	230	900	95

[a] % goethite was calculated from the chemical analysis and does not include excess structural water and residual absorbed water.

https://doi.org/10.1346/CCMN.2009.0570608 Published online by Cambridge University Press

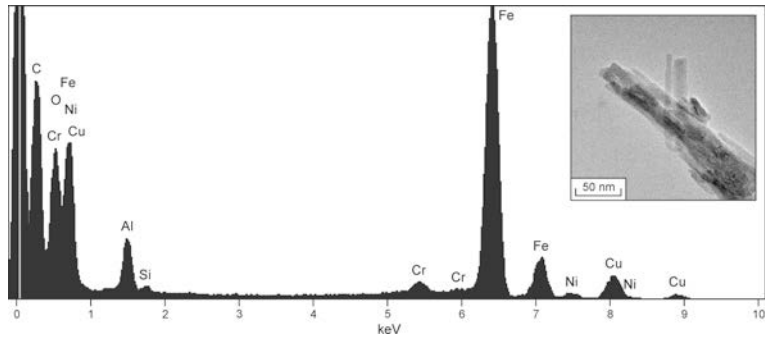

Figure 2. TEM/EDS spectrum of a compound Weda Bay goethite particle (inset). Fe, Al, Cr, and Ni peaks in the spectrum indicate that the metals are associated with goethite. The C, Cu, and Si peaks are from the Si-contaminated, C-coated Cu grids.

electron diffraction (SAED). The instrument, equipped with an Orius 11 Mega pixel digital camera, was optimized for biological imaging (*i.e*. to prevent sample damage from the beam), and was thus highly suitable for goethite which is easily damaged (*i.e.* it dehydroxylates) at high electron beam intensities. Care was taken to prevent dehydroxylation of the goethite crystals under a focused beam. This was accomplished by the use of small apertures, spreading the beam and spending as little time as possible on each crystal within a sample. The SAED images were obtained first with a fully spread beam to prevent dehydroxylation of goethite followed by imaging.

RESULTS AND DISCUSSION

Mineralogy/chemistry of goethites

Goethite was the main constituent identified in the five oxide-type lateritic Ni samples with minor amounts of quartz, talc, maghemite, and kaolinite (Figure 1). Minor amounts of free Mn oxides were detected by transmission electron microscopy/energy dispersive spectrometry (TEM/EDS), but were not detected by XRD analysis. As the samples are mainly composed of goethite they are referred to in this paper as goethites. Chemical analyses of the samples dissolved in 2 M H_2SO_4 and the estimated goethite contents are shown in Table 1. The estimated goethite content does not include excess structural water and residual adsorbed water, as well as insoluble minerals which did not dissolve in 2 M H_2SO_4 (*i.e.* quartz, talc, and chromite which are present in XRD patterns of the residue after dissolution); Table 1 therefore represents mainly goethite chemistry. Kaolinite ($Al_2Si_2O_5(OH)_4$) was identified in the Ravensthorpe and Goro goethites, quartz (SiO_2) in the Weda Bay and Ravensthorpe goethites, maghemite (γ-Fe_2O_3) in the Weda Bay and Kalgoorlie goethites, and talc ($Mg_3Si_4O_{10}(OH)_2$) was a minor impurity in all goethite samples. The Al present (Table 1) is probably associated with substitution of Al^{3+} for Fe^{3+} as is commonly reported for natural goethites (Singh and Gilkes, 1992a). Similarly, goethite is also suggested to be the source of soluble Cr and Ni (Table 1), confirmed by TEM/EDS analysis of goethite crystals (Figure 2, Table 2). Nickel substitution in goethite ranges from 0.84−2.08 wt.%, assuming that all the Ni in the samples is in goethite. The Mn content of the samples is consistent with the presence of minor Mn oxides, which are soluble in H_2SO_4, and these may also contain Ni (*e.g.* Ni-asbolane, Manceau *et al*., 2000).

Dehydroxylation temperature and weight loss due to heating

X-ray diffraction indicates that on heating at 220ºC for 30 min, goethite started to alter to hematite (observed by XRD, Figure 3), which is consistent with thermal analysis results (Figure 4). The hematite/(hematite + goethite) ratio obtained from XRD patterns for all

Table 2. *Me*/(Fe+Me) ratios determined from TEM-EDS spectra of individual crystals of goethite (105ºC).

Sample	Ni/(Fe+Ni)	Al/(Fe+Al)	Cr/(Fe+Cr)	$N^{\#}$
Weda Bay	0.028 (0.005)	0.071 (0.026)	0.018 (0.003)	16
Goro	0.023 (0.009)	0.063 (0.005)	0.045 (0.010)	16
Kalgoorlie	0.027 (0.008)	0.035 (0.012)	0.038 (0.026)	30
Ravensthorpe	0.035 (0.006)	0.000 (0.000)	0.000 (0.000)	12
Koniambo	0.025 (0.010)	0.053 (0.037)	0.016 (0.012)	34

Values in parentheses represent the standard deviation.
$N^{\#}$: number of EDS-TEM spectra measured.

https://doi.org/10.1346/CCMN.2009.0570608 Published online by Cambridge University Press

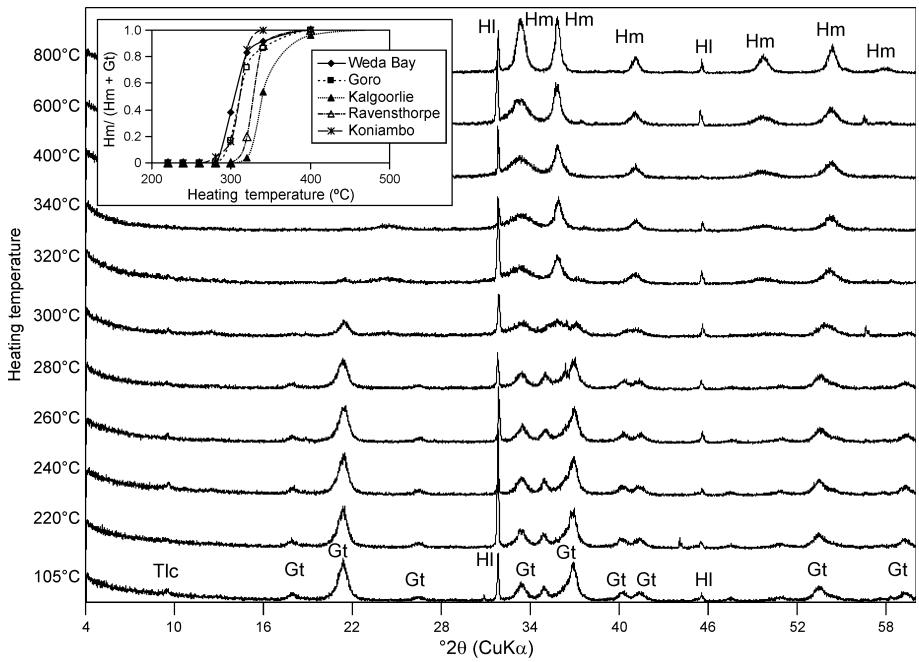

Figure 3. XRD patterns for Goro goethite preheated at various temperatures (105–800ºC for 30 min), with ~10% halite (NaCl) added as an internal standard. Gt = goethite, Hm = hematite including hydrous forms (*i.e.* OH-hematite), Hl = halite, and Tlc = talc. Inset: Hematite/(hematite + goethite) ratio calculated from the integrated intensity of the goethite 110 and hematite 102 reflections for five goethites preheated for 30 min at various temperatures (220–500ºC).

goethites was plotted against heating temperature ranging from 220 to 400ºC (Figure 3 inset). A very broad hematite (012) peak first appears in XRD patterns at preheating temperatures of 300ºC (Weda Bay, Goro and Koniambo) and 340ºC (Kalgoorlie), as illustrated for Goro goethite (Figure 3). No residual goethite was detected by XRD for preheating temperatures above 320ºC (Ravensthorpe) to 400ºC (Kalgoorlie) (*i.e.* absence of goethite 110 peak), with goethite completely altering to well ordered hematite at 800ºC.

Thermal analysis results show that dehydroxylation of goethite is described by a single endotherm between 273ºC (Ravensthorpe) and 286ºC (Kalgoorlie) (Figure 4a–e), indicating a single reaction. Differences in dehydroxylation temperature reflect differences in the amount and type of metal substitution, structural order, and crystal size (Cornell and Schwertmann, 2003). Substitution of Al^{3+} for Fe^{3+} creates local structural sites resembling diaspore (α-AlOOH), which has a dehydroxylation temperature between ~450 and 500ºC (Frost *et al*., 1999). Similarly, substitution of Cr^{3+} for Fe^{3+} creates sites resembling bracewellite (α-CrOOH), which has a dehydroxylation temperature of 440–460ºC (Mackenzie and Berggren, 1970). Al and Cr, therefore, inhibit the dehydroxylation of goethite due to the stronger *Me*–O/OH bond energy than for Fe–O/OH. The substitution of Ni^{2+} for Fe^{3+} has little or no effect on the dehydroxylation temperature of goethite (Wells *et al*., 2006), possibly due to the more complex substitution which involves the coupled substitution of H^+ and Ni^{2+} within goethite to maintain charge neutrality (Carvalho-e-Silva *et al*., 2003). Ravensthorpe goethite dehydroxylates at a slightly lower temperature than the other goethites and contains little or no Al or Cr as shown in the bulk assays (Table 1) and TEM/EDS analyses of single crystals of goethite (Table 2). Wells *et al*. (2006) showed that differences in surface area and crystal size of synthetic metal-substituted goethites were responsible for differences in dehydroxylation temperature. Kalgoorlie goethite dehydroxylates at a higher temperature than the other goethites (285.6ºC), and this does not simply reflect the amount of metals incorporated into the goethite. However, Kalgoorlie goethite has a significantly smaller surface area (27 m^2g^{-1}) than the other goethites (Table 3), which may be the cause of the higher dehydroxylation temperature. A negative linear relationship was observed (Figure 5) between the surface area and the dehydroxylation temperature for the five goethites (R^2 = 0.84).

Values of weight loss due to heating (LOI, 105–800ºC) for goethite samples ranged from 11.6% (Weda Bay) to 15.1% (Kalgoorlie), reflecting to some extent the various amounts of impurities in the goethites (Table 4). Similar results were provided by TG analysis, which showed the weight loss range from 11.4% (Ravensthorpe) to 13.6% (Goro) due to heating between 105 and 800ºC (Table 4, Figure 4). For the remainder of this discussion, therefore, only TGA results are discussed rather than LOI values. For TGA measurements, samples were dried at 105ºC for 10 min to remove

https://doi.org/10.1346/CCMN.2009.0570608 Published online by Cambridge University Press

https://doi.org/10.1346/CCMN.2009.0570608 Published online by Cambridge University Press

Table 3. Surface area and Mean Coherence Length (MCL) values for goethite and hematite calculated from XRD line broadening.

Sample	Heating temperature (ºC)	Hematite						Goethite				Surface area (m^2g^{-1})
		MCL (012) (nm)	MCL (104) (nm)	MCL (110) (nm)	MCL (113) (nm)	MCL (024) (nm)	MCL (116) (nm)	MCL (020) (nm)	MCL (110) (nm)	MCL (111) (nm)	MCL (151) (nm)	
Weda Bay	105							*	10.8	19.5	12.2	59
	220							*	10.8	17.2	13.1	57
	240							*	11.3	13.1	15.1	62
	260							*	10.7	12.8	13.8	65
	280							*	10.4	12.2		76
	300	5.5			7.3		7.4	*				98
	320	6.3	6.1		11.1	7.2	8.2	*				115
	340	4.9	7.5	16.5	15.1	*	9.2					119
	400	5.4	8.9	17.0	11.4	6.5	8.9					116
	600	8.5	9.8	15.6	15.7	7.4	9.3					83
	800	12.8	11.4	20.6	15	11.5	12.2					36
Goro	105							15.9	11.8	12.8	16.2	67
	220							15.5	11.6	12.1	12.6	64
	240							14.3	11.2	12.0	12.4	68
	260							13.0	10.5	11.9	11.7	72
	280							13.3			11.1	76
	300				5.2		6.8					96
	320			14.9	9.2	5.9	8.7					112
	340	5.2	5.5	16.8	12.0	5.6	9.3					125
	400	5.9	6.2	17.1	13.9	5.9	9.8					137
	600	7.3	7.9	17.2	12.5	7.2	10.3					63
	800	13.0	12.3	20.6	15.4	12.5	13.1					32
Kalgoorlie	105							15.7	12.7	16.6	14.2	27
	220							19.9	12.4	18.2	14.6	28
	240							15.8	13.2	17.2	14.5	28
	260							13.0	11.4	18.5	14.9	29
	280											29
	300								11.6		11.8	31
	320						8.1		11.5			41
	340	5.9	8.1	20.8	9.7	5.4	8.2					62
	400	6.4	6.7	22.4	14.3	6.7	9.9					71
	600	8.6	8.8	18.5	14.0	7.8	11.2					49
	800	21.4	19.8	26.5	27.1	17.7	21.0					10

https://doi.org/10.1346/CCMN.2009.0570608 Published online by Cambridge University Press

	105							15.9	14.3	19.4	12.6	76
	220							13.6	14.8	19.3	13.0	81
	240							12.4	22.2	15.2	13.0	83
	260							11.5	19.1	15.0	12.4	83
	280							13.1		15.5	13.5	83
Ravensthorpe	300							12.7		15.0	13.0	113
	320	*	6.5	8.8	9.5	*	7.7	12.4				108
	340	4.4	6.9	16.9	19.7	*	9.4					117
	400	4.8	6.3	14.2	19.3	*	10.4					115
	600	5.2	7.0	14.2	27.4	*	10.9					80
	800	10.3	11.0	17.8	21.5	*	14.7					30
	105							15.2	10.5	12.9	12.8	83
	220							16.8	10.3	20.5	11.0	82
	240							16.2	10.8	19.5	10.4	85
	260								10.0	14.8	10.9	85
	280							9.2		11.6		94
Koniambo	300				5.8			11.1				104
	320	6.3	6.5	15.9	9.9	6.9	8.0	8.3				124
	340	5.4	6.5	18.0	11.5	7.2	9.6					138
	400	4.9	6.6	17.3	11.8	5.2	8.6					125
	600	7.8	7.8	19.3	12.3	7.8	8.7					70
	800	15.2	14.5	19.8	17.1	14.1	13.3					34

* denotes reflections that could not be resolved due to overlapping reflections.

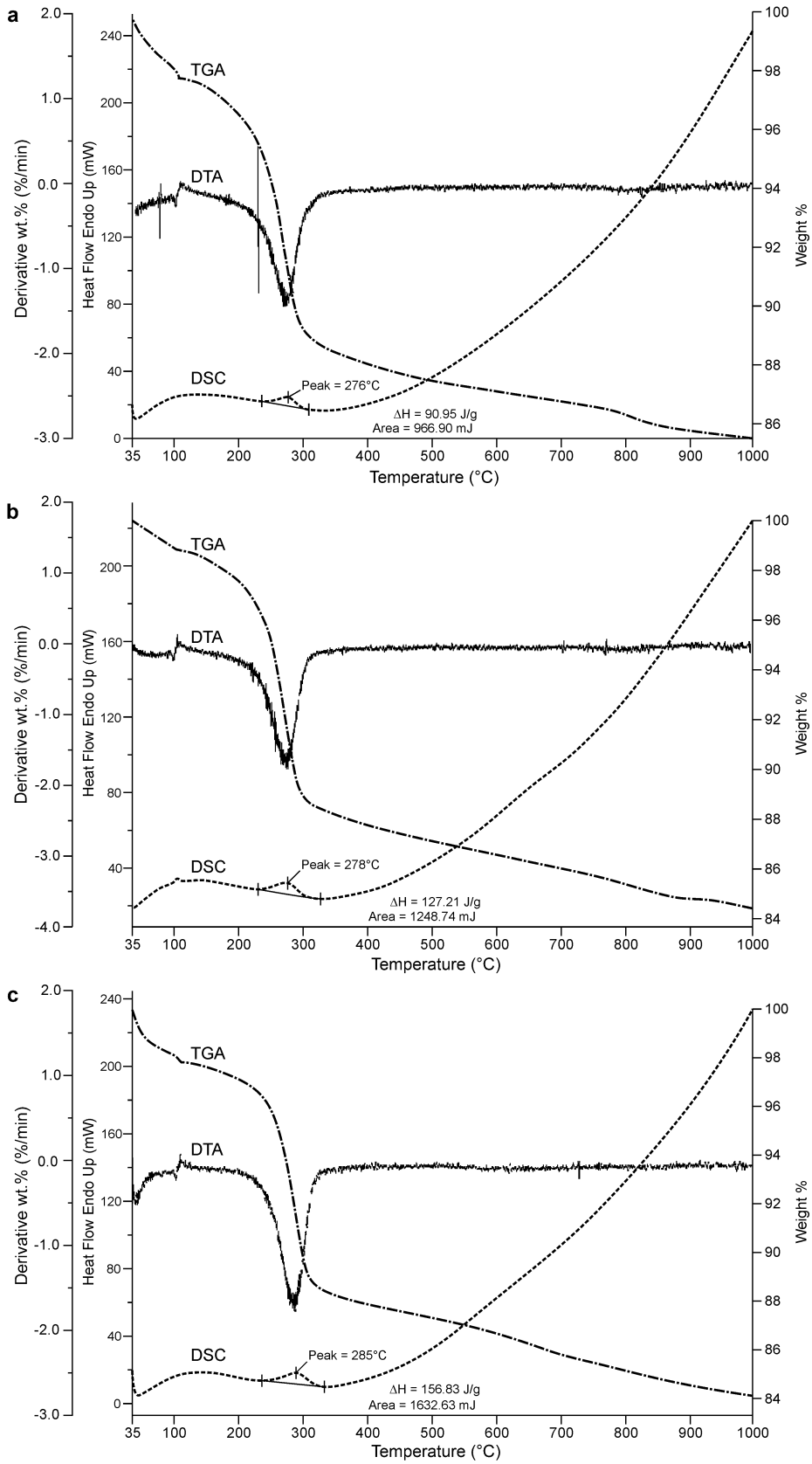

https://doi.org/10.1346/CCMN.2009.0570608 Published online by Cambridge University Press

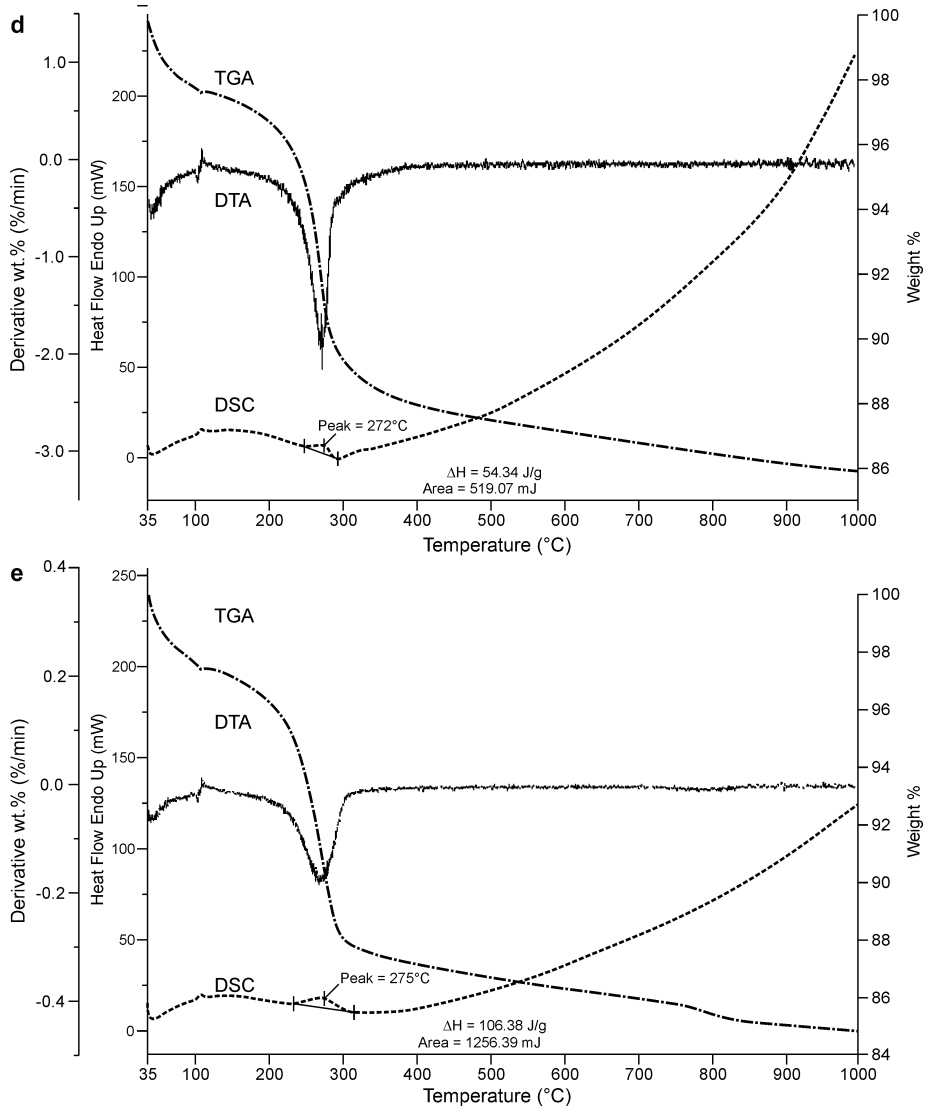

Figure 4 (*facing page and above*). DTA/TGA and DSC curves for goethite from: (a) Weda Bay; (b) Goro; (c) Kalgoorlie; (d) Ravensthorpe; and (e) Koniambo.

adsorbed water. Weight-loss measurements from TGA over the temperature range 105–400ºC, therefore, mostly represent the loss of structural water (*i.e.* bound OH^-) from goethite. The weight loss of 10.0% (Ravensthorpe) to 11.4% (Goro) on heating to 400ºC (*i.e.* alteration to OH-hematite) is similar to the theoretical loss of structural H_2O for ideal goethite (*i.e.* 10.1%):

$$2[Fe^{3+}O^{2-}(OH^-)] \rightarrow Fe_2^{3+}O_3^{2-} + H_2O \qquad (1)$$

On further heating (400–1000ºC), an additional weight loss of 1.8% (Ravensthorpe) to 3.3% (Kalgoorlie) associated with the complete dehydroxylation of goethite was observed. This additional weight loss may be due to the loss of excess structural OH^- associated with: (1) minor impurities (*i.e.* kaolinite); and

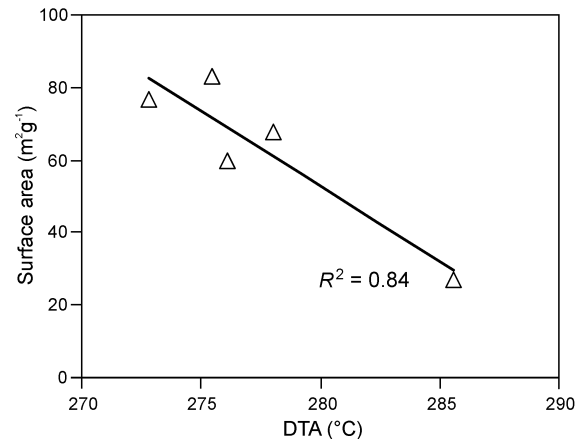

Figure 5. Linear negative relationship between initial surface area (*i.e.* prior to heating) and dehydroxylation temperature (from DTA results) ($R^2 = 0.84$) for goethite.

https://doi.org/10.1346/CCMN.2009.0570608 Published online by Cambridge University Press

Table 4. Summary of weight loss values from TG analysis and LOI for all goethites.

Sample	TGA analysis % weight loss				% weight loss assuming pure goethite samples		DTA (ºC)	Loss on ignition (LOI) results		
	105–400ºC	400–800ºC	800–1000ºC	Total (up to 1000ºC)	Total	Total minus ideal goethite value		105–400ºC	400–800ºC	Total 105–800ºC
Weda Bay	10.05	1.60	0.75	12.40	19.40	9.30	276	11.61	0.03	11.64
Goro	11.40	2.15	0.95	14.50	20.70	10.60	278	9.76	4.88	14.64
Kalgoorlie	10.50	2.70	0.60	13.80	19.40	9.30	285	9.81	5.26	15.07
Ravensthorpe	10.04	1.40	0.36	11.80	19.00	8.90	272	9.29	2.81	12.10
Koniambo	10.55	1.80	0.35	12.70	14.60	4.50	275	9.65	3.17	12.82

(2) coupled substitution with divalent metals (*e.g.* Ni^{2+}), which compensates for cation-charge deficiency (Ruan and Gilkes., 1995; Ruan *et al*., 2002). The theoretical weight-loss contribution from kaolinite dehydroxylation in these samples, which occurs at ~550ºC, is calculated to be ~0.35% (*i.e.* assuming 2.5% kaolinite impurity for Ravensthorpe goethite, Figure 1). The dehydroxylation process is not observed, however, in the thermal analysis results (Figure 4d), and is not applicable to the other goethites as they contain little or no kaolinite. The contribution from divalent metal substitution in goethite is more significant. For example, theoretical dehydroxylation for goethite containing 10 mol.% Ni of formula $Fe^{3+}_{0.9}Ni^{2+}_{0.1}O^{2-}_{0.9}(OH^{-})_{1.1}$ is as follows:

$$2[Fe^{3+}_{0.9}Ni^{2+}_{0.1}O^{2-}_{0.9}(OH^{-})_{1.1}] \rightarrow (Fe^{3+}_{0.9}Ni^{2+}_{0.1}H^{+}_{0.1})_2O^{2-}_3 + H_2O \quad (2)$$

The theoretical loss of weight due to H_2O is 10.1% for 10 mol.% Ni-substituted goethite (*i.e.* the same as for pure goethite). This equation assumes, however, that Ni and associated H^+ are fully retained in the neo-formed hematite structure. Acid dissolution experiments for the same goethite samples analysed in this paper showed that some Ni is exsolved from hematite by heating at 600–800ºC and may reside on the surface of neoformed hematite crystals as a discrete (*i.e.* NiO) phase (Landers *et al.* 2008). The following equation may provide a more appropriate description of the dehydroxylation reaction:

$$2[Fe^{3+}_{0.9}Ni^{2+}_{0.1}O^{2-}_{0.9}(OH^{-})_{1.1}] \rightarrow 0.9(Fe^{3+}_2O^{2-}_3) + 0.2Ni^{2+}O^{2-} + 1.1H_2O \quad (3)$$

The theoretical loss of weight due to H_2O evolution is now 11.1% for 10 mol.% Ni-substituted goethite as opposed to 10.1% for unsubstituted goethite. On this basis, goethite containing ~3 mol.% of Ni (*i.e.* a typical lateritic Ni goethite) would experience an additional loss in weight of ~0.3 wt.%, which is much less than the observed additional average loss of 2.94%. Unit-cell volume measurements for hematite (Figure 6c) also provide evidence to suggest that the weight loss due to heating above 400ºC is not a result of loss of bound OH^- units, as no further contraction of the unit-cell volume at temperatures above 400ºC is possible. The remaining weight loss (~5–10% assuming pure goethite; Table 4) may be due to: (1) free water trapped in pores formed during dehydroxylation, which is released at higher temperatures as volume diffusion enables hematite crystals to develop a nonporous fabric (Pomiès *et al*., 1999); or (2) water associated with poorly ordered Fe oxide phases that were not detected by XRD. Torrent *et al*. (1992) showed that poorly ordered ferrihydrite impurities in New Caledonian Fe oxide samples contained up to 20% of water.

Unit-cell dimensions

The unit-cell dimensions (*a*, *b*, and *c* axes) of the goethites are similar except for Ravensthorpe goethite,

https://doi.org/10.1346/CCMN.2009.0570608 Published online by Cambridge University Press

which has considerably larger unit-cell dimensions than the other four goethites (Figure 7a–d). The larger unit cell of Ravensthorpe goethite may be due *inter alia* to: (1) the relatively small levels of Cr and Al incorporated in this goethite; and (2) the large amount of Ni in this goethite compared to the other goethites (Table 2). Previous authors reported a systematic decrease in the unit-cell dimensions of synthetic goethite with increasing substitution of Al and Cr and an increase with increasing Ni (coupled with H^+) substitution (Gerth, 1990; Manceau *et al*., 2000; Ruan *et al*., 2002; Carvalho-e-Silva *et al*., 2003; Wells *et al*., 2006). Replacement of

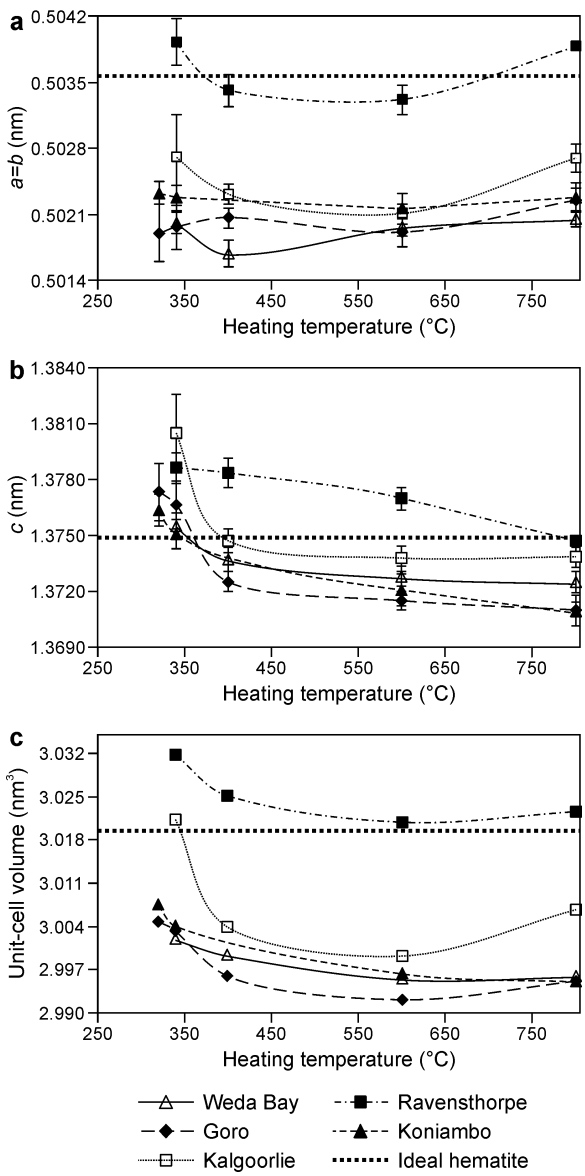

Figure 6. Unit-cell parameters for hematite *vs.* pre-heating temperature. (a) *a* and *b* dimensions; (b) *c* dimension; (c) unit-cell volume. Ideal hematite values (dashed lines) are taken from card 33-664 (JCPDS, 1988).

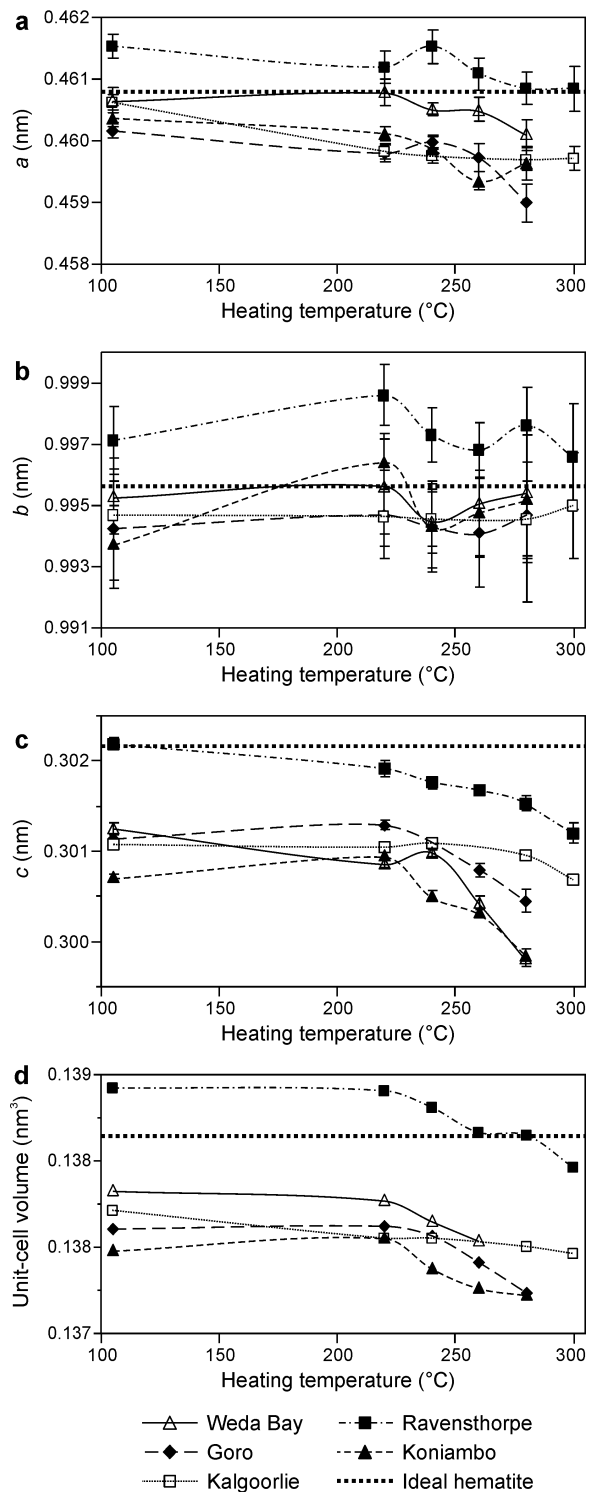

Figure 7. Unit-cell parameters for goethite *vs.* pre-heating temperature: (a) *a* dimension; (b) *b* dimension; (c) *c* dimension; (d) goethite unit-cell volume. Ideal goethite values (dashed lines) are taken from card 29-713 (JCPDS, 1988).

https://doi.org/10.1346/CCMN.2009.0570608 Published online by Cambridge University Press

Fe^{3+} (ionic radius, *r* of 0.0645 nm) by the smaller Al^{3+} (*r* = 0.0535 nm) and Cr^{3+} (*r* = 0.0615 nm) ions in the goethite structure is consistent with reductions in the unit-cell dimensions in the direction of the isostructural end-members diaspore (α-AlOOH) and bracewellite (α-CrOOH), respectively. Results of X-ray absorption spectroscopy (XAS) analysis showed $NiO_2(OH)_4$ octahedra replacing $FeO_3(OH)_3$ octahedra (Carvalho-e-Silva *et al*., 2003), a contraction of the goethite structure in the plane of edge-sharing double chains and expansion in the direction of corner linkages with increasing Ni substitution (Manceau *et al*., 2000). More recently Carvalho-e-Silva *et al.* (2003) used XAS analysis to show that the polyhedral linkages of Ni-substituted goethite are similar to those in pure goethite (*i.e.* edge-sharing linkages of Fe and Ni in pure goethite were essentially the same). However, the third and longest metal–metal distance was greater for Ni (3.7 Å) than the expected corner-sharing distance of Fe (3.46 Å), indicating that incorporation of Ni locally dilates the structure, resulting in an increase in unit-cell volume with increased incorporation of Ni^{2+} (Wells *et al*., 2006).

The incorporation of cations other than Ni, Al, and Cr into goethite (*e.g.* Mn, Co, V, Ti, Mg, and Ba) also affects unit-cell lengths (Gerth, 1990; Schwertmann and Pfab, 1996; Manceau *et al*., 2000; Wells *et al*., 2006). However, the very small amounts of these metals detected in the bulk goethite assay (<1 wt.% total, Table 1) would not be sufficient to significantly affect goethite unit-cell dimensions. Similarly, these metals were not detected by TEM/EDS analysis of individual goethite crystals (Figure 2, Table 2).

The goethite unit-cell *a* and *b* dimensions remained almost constant with increasing preheating temperature for all goethites (Figure 7a,b), while the *c* unit-cell dimension and, thus, the unit-cell volume decreased significantly (Figure 7c,d). The decrease in the unit-cell *c* direction with increasing temperature is consistent with reported observations (Gualtieri and Venturelli, 1999; Wells *et al*., 2006). In contrast to the present data, Gualtieri and Venturelli (1999) reported small systematic increases in the *a* and *b* unit-cell dimensions with increasing temperature. The differences may be due to: (1) the present goethites being substituted with multiple cations (and accompanying substitution of H^+ to retain charge neutrality where divalent metals are present), which may influence the effects of heating on the *a* and *b* dimensions; (2) the lower precision of the XRD method used in this study compared to the more precise synchrotron XRD results of Gualtieri and Venturelli (1999); or (3) synthetic goethites may differ in behavior from natural goethites. The large decrease in the *c*-axis dimension due to heating observed by all authors may be a result of the vacancy generated by proton migration from the goethite structure during dehydroxylation. Initially, proton retention was for charge balance due to the partially dehydroxylated goethite phase (*i.e.* OH-hematite) being Fe deficient (Gualtieri and Venturelli, 1999). Movement of Fe atoms closer together along the *c* axis at greater heating temperatures fills this vacancy. In addition, for the present goethites, proton retention for charge balance due to divalent metal substitution also contributes to this proton migration on heating and subsequent contraction in the *c*-axis dimension.

The unit-cell size of neoformed OH-hematite decreased with increasing heating temperature up to ~400ºC and at higher temperatures (well ordered hematite) this size remained constant or decreased slightly (except for Ravensthorpe goethite for which the hematite *c* value continued to decrease up to 800ºC) (Figure 6). The *a*=*b* unit-cell length initially decreased with increasing heating temperature to ~600ºC and then increased up to 800ºC (Figure 6a,b). The trends are reflected in values of hematite unit-cell volume, which decreased with increasing temperature up to 600ºC followed by a slight increase at 800ºC (except for Koniambo) (Figure 6c). The decrease in the unit-cell volume of hematite is consistent with the results of previous authors who have shown that the unit cell of disordered hematite, formed at low dehydroxylation temperatures (~340ºC, OH-hematite), appears to be ~0.3% larger than for well ordered hematite, possibly due to the presence of structural hydroxyl (Brown, 1980). Changes in the hematite unit-cell volume with increasing temperature are suggested to reflect the loss of residual water (OH^-) from partially dehydroxylated goethite (or neoformed OH-hematite) and rearrangement of Fe^{3+} with a consequent decrease in the size of the unit cell as well ordered hematite started to form at >600ºC. The slight increase in hematite unit-cell volume for samples heated at 800ºC reflects expansion of the unit cell of well ordered hematite in the *ab* plane. This may be in response to increased structural ordering (*i.e.* sharp XRD peaks, Figure 3) of hematite at 800ºC.

XRD line broadening/mean coherent length (MCL)

Non-instrumental XRD line broadening is caused by small crystal size, including nm-sized twinning and structural disorder in partially dehydroxylated goethite (*i.e.* OH-hematite) and neoformed hematite (Cornell and Schwertmann, 2003). Structural disorder in OH-hematite (~340ºC) is due, *inter alia*, to the presence of obverse and reverse twin formation (Lima de Faria, 1963; Watari *et al*., 1979). The twins are due to two arrangements of Fe ions within the same oxygen framework (*i.e.* obverse and reverse). During goethite dehydroxylation the hexagonal, close-packed oxygen sequence is retained. However, Fe in the sub-lattice may adopt one of two non-preferred stacking sequences (*i.e.* causing fine twinning in hematite) (Lima de Faria, 1963; Watari *et al*., 1979; Löffler and Mader, 2006). The structural disorder in OH-hematite is clearly seen in the greater broadening of some reflections where $h-k = 3n$ and $l \neq 3n$ (*e.g.* 012, 104, and 024) (Figure 8), relative to

https://doi.org/10.1346/CCMN.2009.0570608 Published online by Cambridge University Press

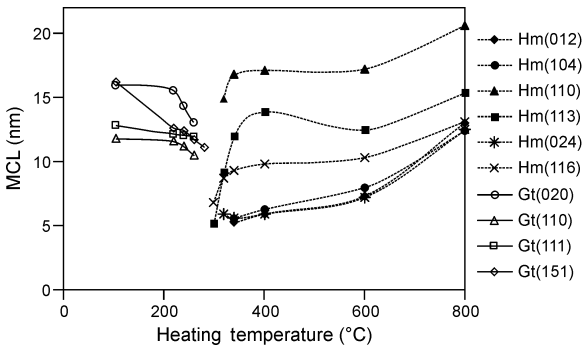

Figure 8. Mean coherent length (MCL) calculated from FWHM values for goethite (Gt) and hematite (Hm) reflections for Goro goethite preheated for 30 min at various temperatures (105–800ºC). The goethite 110 and 020 reflections are approximately directionally equivalent to the hematite 116 and 110 reflections, respectively.

reflections where $l = 3n$ (*e.g.* 110 and 113 reflections) which are sharper (Figure 9). The hematite (116) reflection is associated with both the Fe stacking sequences; hence, line broadening is intermediate (Figure 9).

Mean coherent length (MCL) data, calculated using the Scherrer formula (Klug and Alexander, 1974), for goethite and hematite are presented in Table 3. For the original (105ºC) goethite, MCL_{110} was between 10.5 (Koniambo) and 14.3 nm (Ravensthorpe) and goethite MCL_{111} varied from 12.8 (Goro) to 19.5 nm (Weda Bay) (Table 3). These values are similar to those found by previous authors for goethite in New Caledonian soils, which includes the Goro and Koniambo lateritic nickel deposits (*e.g.* 14 and 33 nm, Schwertmann and Latham, 1986; 24 and 22 nm, Perrier *et al*., 2006; and 14.7 and 19.8 nm, Landers and Gilkes, 2007), for the 110 and 111 reflections, respectively. Singh and Gilkes (1992a) reported values of goethite MCL_{110} and MCL_{111} of ~20 nm for mostly lateritic soils from SW Australia. Variations in MCL may be due to the amounts and species (*e.g.* Cr, Al, and Ni) of cations incorporated into goethite, which affect crystal size and order (Lim-Nunez, 1985; Ruan and Gilkes, 1995; Wells *et al*., 2006).

For all the samples an increase in hematite MCL_{110} (*e.g.* Koniambo, 15.9–19.8 nm) and MCL_{104} (*e.g.* Koniambo, 6.5–14.5nm) was observed with increasing temperature up to 800ºC (Table 3, Figure 8). Perrier *et al.* (2006) and Landers and Gilkes (2007) reported similar values for heated (2 h at 600ºC) goethitic soils from Koniambo.

Comparison of MCL values for approximately directionally equivalent goethite and hematite MCL values (*i.e.* goethite 110 reflection *vs.* the hematite 116 reflection; goethite 020 reflection *vs.* the hematite 110 reflection) indicates that the newly formed hematite crystals are larger than precursor goethite crystals. Ruan and Gilkes (1995) reported similar results and suggested that regularly ordered hematite domains develop from adjacent goethite crystals by sintering and surface diffusion, thus forming larger crystals at high temperatures.

The MCL values for the hematite 104, 012, and 024 reflections increased substantially (~2 to 3 fold) with increasing heating temperature (300–800ºC) while the MCL for the hematite 110 reflection remained relatively constant (<2-fold increase) (Table 3, Figure 8). Other authors reported similar results (Rooksby, 1961; Brown, 1980; Lim-Nunez, 1985; Landers and Gilkes, 2007). The hematite 104 reflection, which is an approximate

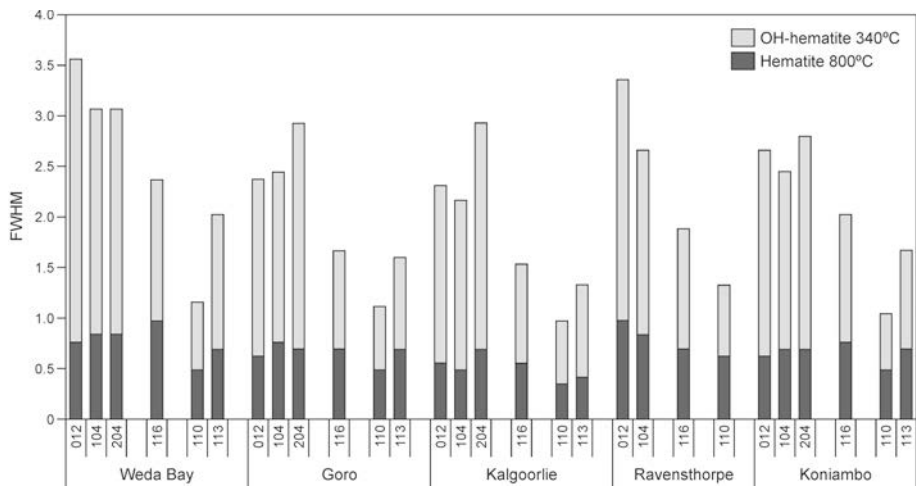

Figure 9. Full width at half maximum (FWHM) of XRD reflections for hematite in goethites heated at 340ºC (OH-hematite) and 800ºC (hematite). The measurements are for hematite reflections where $h-k = 3n$ and $l \neq 3n$ (012, 104, and 204), those for $l = 3n$ (110 and 113), and for the reflection associated with both the Fe stacking sequences (116). Peak broadening is much greater for partially dehydroxylated goethite (OH-hematite) compared to well ordered hematite, and for reflections where $h-k = 3n$ and $l \neq 3n$. The values have not been corrected for line broadening due to experimental configuration.

https://doi.org/10.1346/CCMN.2009.0570608 Published online by Cambridge University Press

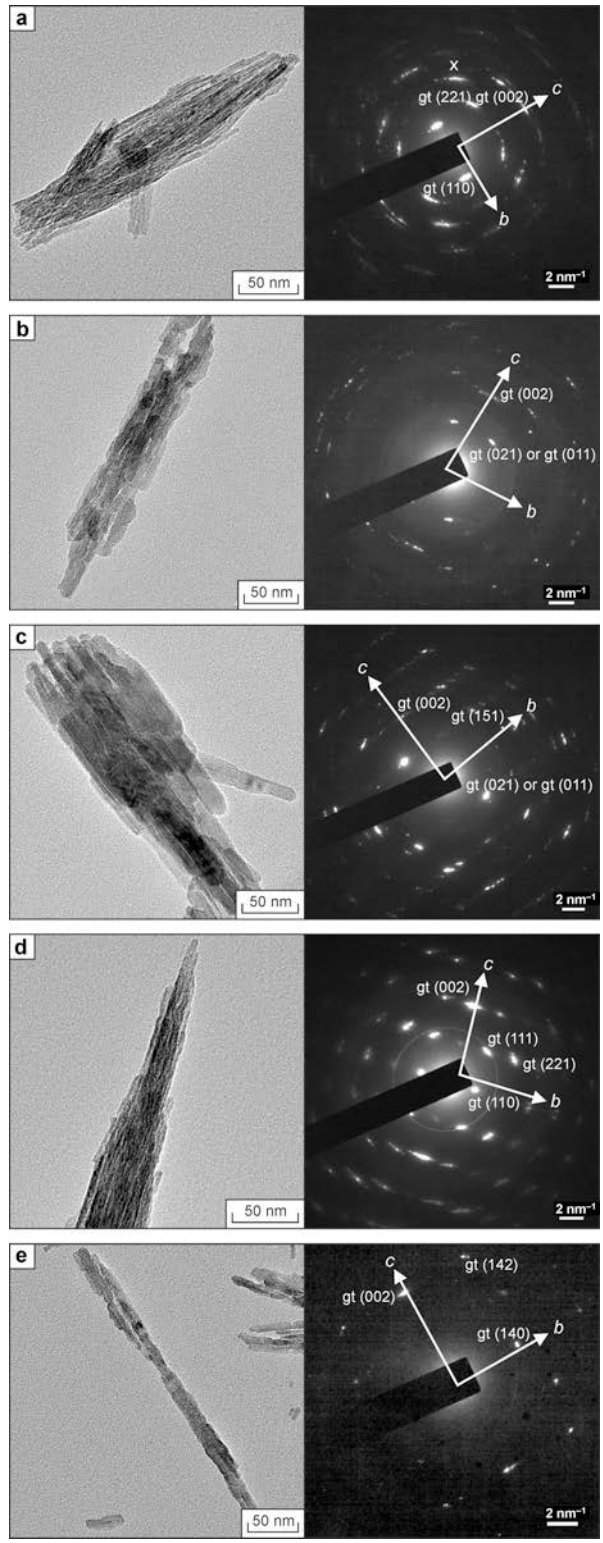

Figure 10. TEM images and accompanying SAED patterns in the correct orientation for compound particles consisting of rafts of acicular goethite crystals from (a) Weda Bay, (b) Goro, (c) Kalgoorlie, (d) Ravensthorpe, and (e) Koniambo. The SAED patterns indicate that the goethite crystals are elongated along the *c*-axis direction. The letter x (micrograph a) shows the arcing of spots in diffraction patterns indicating that the acicular crystals in the rafts are not in perfect parallel alignment.

https://doi.org/10.1346/CCMN.2009.0570608 Published online by Cambridge University Press

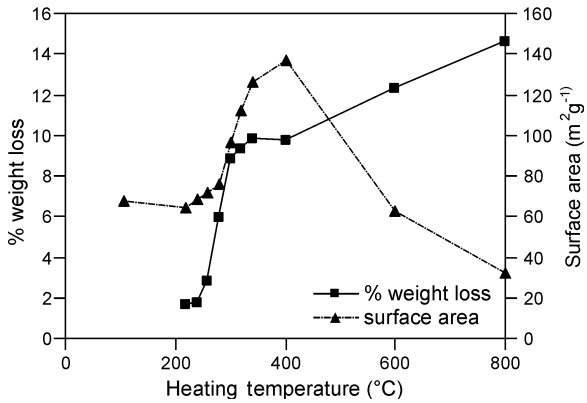

Figure 11. Surface area and % weight loss for Goro goethite on heating at various temperatures (105–800ºC).

measure of crystal size along the *c* axis, is much broader than for the 110 reflection which is due to the organization of twin domains associated with the two different orderings of Fe. Partially dehydroxylated goethite (*i.e.* OH-hematite) inherits a structural subunit ($Fe(OH)_2$) (Francombe and Rooksby, 1959) common to both goethite and hematite which preserves an ordered structure along the hematite *a*-axis direction. The structure along the *c*-axis direction for hematite differs considerably from that for goethite. Consequently, high temperatures (~800ºC) are needed to enable the development of a regular structure along the *c*-axis direction of hematite (*i.e.* formation of well ordered hematite). During this transformation, retained water is gradually lost (Figure 4) and both Fe and substituted cations are rearranged.

Surface area

The surface area of the five goethites ranged between 27 m^2g^{-1} (Kalgoorlie) and 83 m^2g^{-1} (Koniambo) (Table 3). The surface area of Kalgoorlie goethite is considerably smaller than the other goethites due to the larger size and more regular shapes of the Kalgoorlie goethite crystals. The results appear to be inconsistent with the MCL values for the Kalgoorlie goethite, which were similar to those of the other goethites. However, MCL is a measure of diffraction length (*i.e.* coherently diffracting length) and not of particle size which strongly influences surface area. Particles of goethite may contain several discrete diffracting zones so that MCL values will be smaller than individual particles. Values of MCL_{110} and MCL_{113} for the neo-formed Kalgoorlie hematite were larger than for other neo-formed hematites, presumably because the multiple diffracting zones of goethite coalesced into larger hematite crystals compared to other samples. Examination by TEM supports this assertion and showed that Kalgoorlie goethite crystals have smoother surfaces with fewer imperfections compared to other goethites (Figure 10c).

Surface areas for the other goethites are comparable to those found by Landers and Gilkes (2007) (74 m^2g^{-1}) and Schwertmann and Latham (1986) (57–139 m^2g^{-1}) for New Caledonian goethites. No substantial change was observed in surface area of the goethites on heating until ~240–300ºC (*i.e.* transformation of goethite to OH-hematite) (Figure 11). From this point the surface area increased dramatically (~2-fold) with increasing heating temperature until all the goethite had transformed into OH-hematite (340–400ºC). This was followed by a decrease in surface area on heating to 800ºC. The trend reflects the development of micropores in OH-hematite at 240–300ºC due to the partial dehydroxylation of goethite with expulsion of structural water into lamella pores and is consistent with TEM analysis of newly formed hematite. Removal of these pores with further heating (up to 800ºC) by surface and volume diffusion,

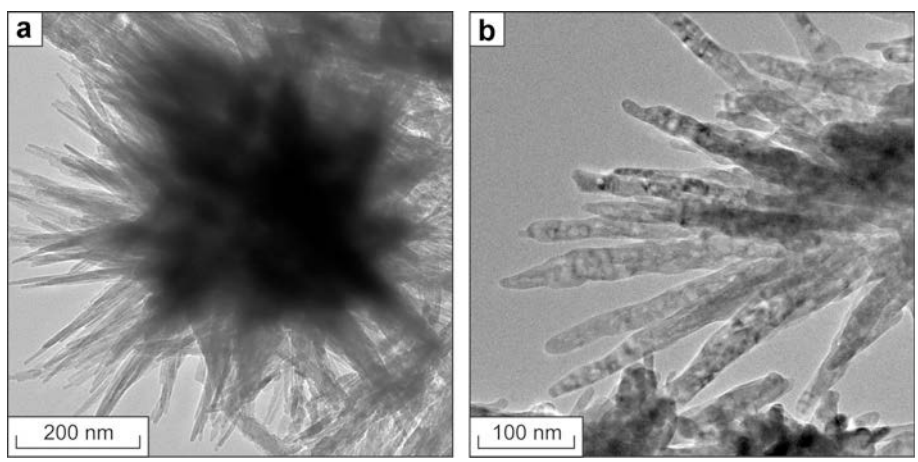

Figure 12. TEM images of an echidna-shaped aggregate of acicular crystals for (a) Goro goethite at 105ºC, and (b) hematite formed at 800ºC from Goro goethite. The echidna-shaped particle morphology is retained by hematite although the acicular crystals have developed rounded terminations.

https://doi.org/10.1346/CCMN.2009.0570608 Published online by Cambridge University Press

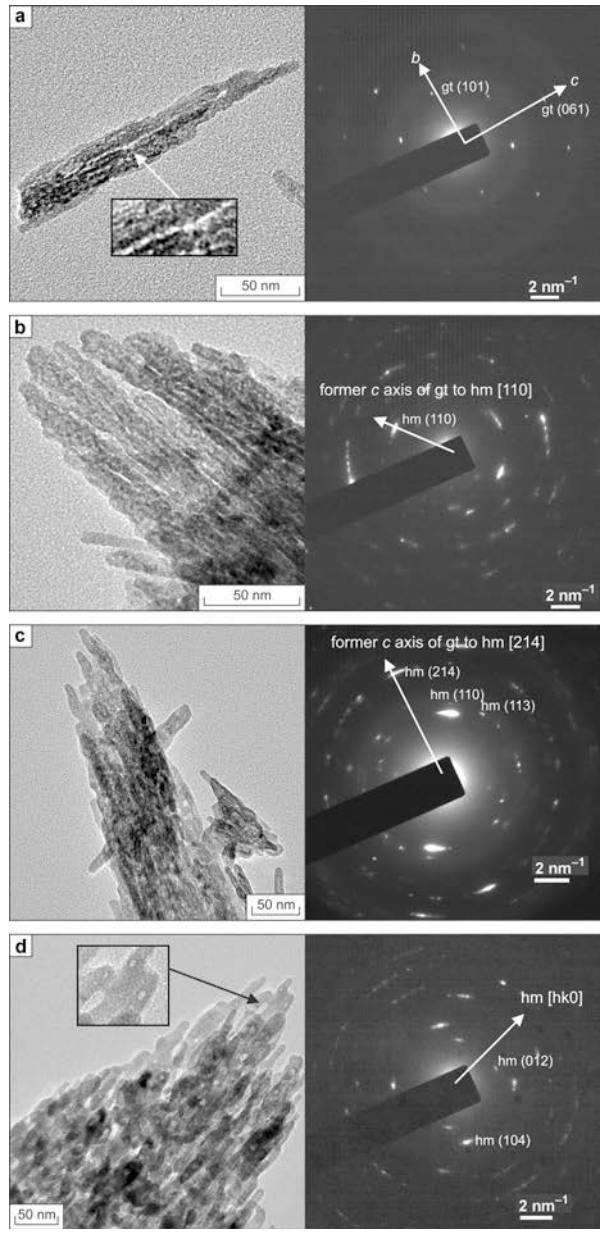

Figure 13. TEM images and accompanying SAED patterns in correct orientation of complex raft-like aggregates of crystals in Goro goethite heated at (a) 300ºC, (b) 400ºC (OH-hematite), (c) 600ºC (hematite), and (d) 800ºC (hematite). The arrow in micrograph (a) (and inset) indicates a slit-shaped micropore extending the length of the particle and in micrograph (d) (and inset) the arrow indicates a residual, elliptically shaped micropore preserved in the raft-like assemblage of well ordered hematite crystals. Arrows in the SAED patterns indicate the axis of elongation, with goethite elongated along the *c* axis and hematite elongated along the [110] axis. The SAED patterns of hematite are not a simple (*hk*0) network of reflections due to the hematite crystals being slightly inclined to the grid so that (*hkl*) reflections occur.

and associated formation of well ordered hematite crystals (Watari *et al*., 1982), decreased surface area. The surface area of hematites formed at 800ºC was between 10.4 m^2g^{-1} (Kalgoorlie) and 36.1 m^2g^{-1} (Weda Bay), which is approximately half the surface area of the original goethites. These results are similar to those reported by Schwertmann and Latham (1986) where the surface area of hematite was between 62 and 82 m^2g^{-1}. The present values are smaller than for heated Boulinda and Tiebaghi massif (New Caledonia) goethites. Landers and Gilkes (2007) reported that the surface area of hematite (101 m^2g^{-1}) produced by heating Koniambo goethite at 600ºC for 2 h was larger than for the original goethite (74 m^2g^{-1}).

https://doi.org/10.1346/CCMN.2009.0570608 Published online by Cambridge University Press

Crystal morphology

Transmission electron microscopy showed that all goethites have mainly acicular or lathlike crystal morphology with most crystals being aggregated into raft-like particles (*e.g.* Figure 10a). The acicular crystals vary considerably in length (~20–400 nm) and width (~10–30 nm) between goethite samples, and within each goethite sample, thus making it difficult to quantify crystal size. Selected area electron diffraction (SAED) of single goethite crystals indicated that the *a* axis is parallel to the electron beam and the goethite crystals are elongated along the *c*-axis direction (Figure 10a–e) (Cornell *et al*., 1983; Wells *et al*., 2006). The acicular crystals occur in three assemblages (*i.e.* different growth forms) including: (1) single crystals (*e.g.* Figure 10e); (2) compound particles (*i.e.* parallel crystals) or rafts (*e.g.* Figure 10a); and (3) echidna-shaped, three dimensional radiating arrays of crystals (Figure 12a). For compound particles, each crystal is slightly misoriented with respect to its neighbors (Cornell and Schwertmann, 2003). The SAED patterns show distinct arcing of reflections representing this range of orientation (*e.g.* Figure 10a–d). The 3D radiating arrays (*i.e.* echidna-shaped) may consist of a hematite nucleus with outgrowths of acicular goethite on all hematite faces (Barrón *et al*., 1997). The number of acicular crystals present in rafts and echidna-shaped particles varies considerably. For example, for the Goro goethite, between two and thousands of crystals are present per particle.

Substitution of metals into goethite may affect crystal morphology, *e.g.* with increasing Al substitution, multicrystal arrangements increase and crystal width decreases (Schulze and Schwertmann, 1984) by retarding growth along the *c*-axis direction (Schulze and Schwertmann, 1984; Ruan *et al*., 2002). Due to the multi-crystalline character of many goethite particles, crystal width (in the *b*- and *c*-axis directions) measured from XRD line-broadening values does not match particle sizes observed in TEM images. Values of MCL represent a measurement of crystallite size rather than particle size. The aggregated nature of goethite particles affects the kinetics of acid dissolution (Landers *et al*., 2008) as much initial dissolution occurs at intercrystal boundaries, which increases surface area, thereby facilitating increased protonation of the crystal surface (*i.e.* larger surface area for acid attack) and an increase in dissolution rate.

Changes in particle morphology associated with the alteration of Goro goethite to hematite due to heating are shown in Figure 13; similar changes occurred for all goethites but are not shown here. In most circumstances the acicular morphology of crystals and the various aggregate fabrics of goethite are retained throughout the recrystallization process (105–800ºC) (Figure 12b, 13). However, at higher temperatures, needles coalesce and surface diffusion occurs, forming rounded crystals of hematite (Figure 14).

Aggregates of goethite crystals heated at 300ºC contain many elongated pores. Initially the pores appear to be irregularly slit shaped (at 300ºC) and may extend along the *c* axis for the entire length of the crystal (Figure 13a). At this point (*i.e.* 300ºC), XRD and SAED indicate that goethite is the dominant Fe oxide present (Figure 13a). For temperatures up to 340–400ºC (*i.e.* OH-hematite), these slit shaped pores persist and a few elliptical shaped micropres are present (Figure 13b). These observations are consistent with those obtained by Pomiès *et al*. (1999) and Löffler and Mader (2006) for synthetic goethites. For samples preheated at 400ºC, SAED patterns indicate that goethite no longer exists and the former *c* axis of goethite is now the 110 axis of hematite (Figure 13b). For temperatures of 600 and 800ºC, the elongated micropores mostly disappear and fewer elliptical micropores (up to 10 nm) persist (Figure 13d). The residual micropores are suggested to contain free water vapor trapped in the neoformed hematite structure. The hematite crystals have rounded ends (Figure 13c,d) and are mostly larger than the precursor goethite crystals, reflecting the coalescing of hematite crystals with increasing heating temperature (Figure 13d). High-resolution TEM imaging shows that the lattice fringes of hematite extend across the former boundaries between precursor goethite crystals, which indicates that the crystal domains have coalesced into single grains by sintering and volume diffusion resulting in larger particles (Figure 15). Arcing of the hematite 300 spot in SAED patterns (Figure 15d) of large aggregations of hematite crystals (including Figure 15a–c) indicates that the hematite crystals are

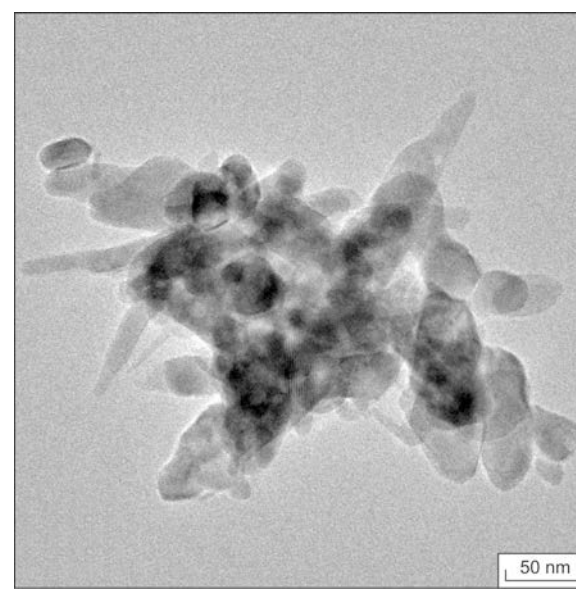

Figure 14. TEM image of Kalgoorlie goethite heated at 800ºC (hematite) showing both rounded and lathlike crystals.

https://doi.org/10.1346/CCMN.2009.0570608 Published online by Cambridge University Press

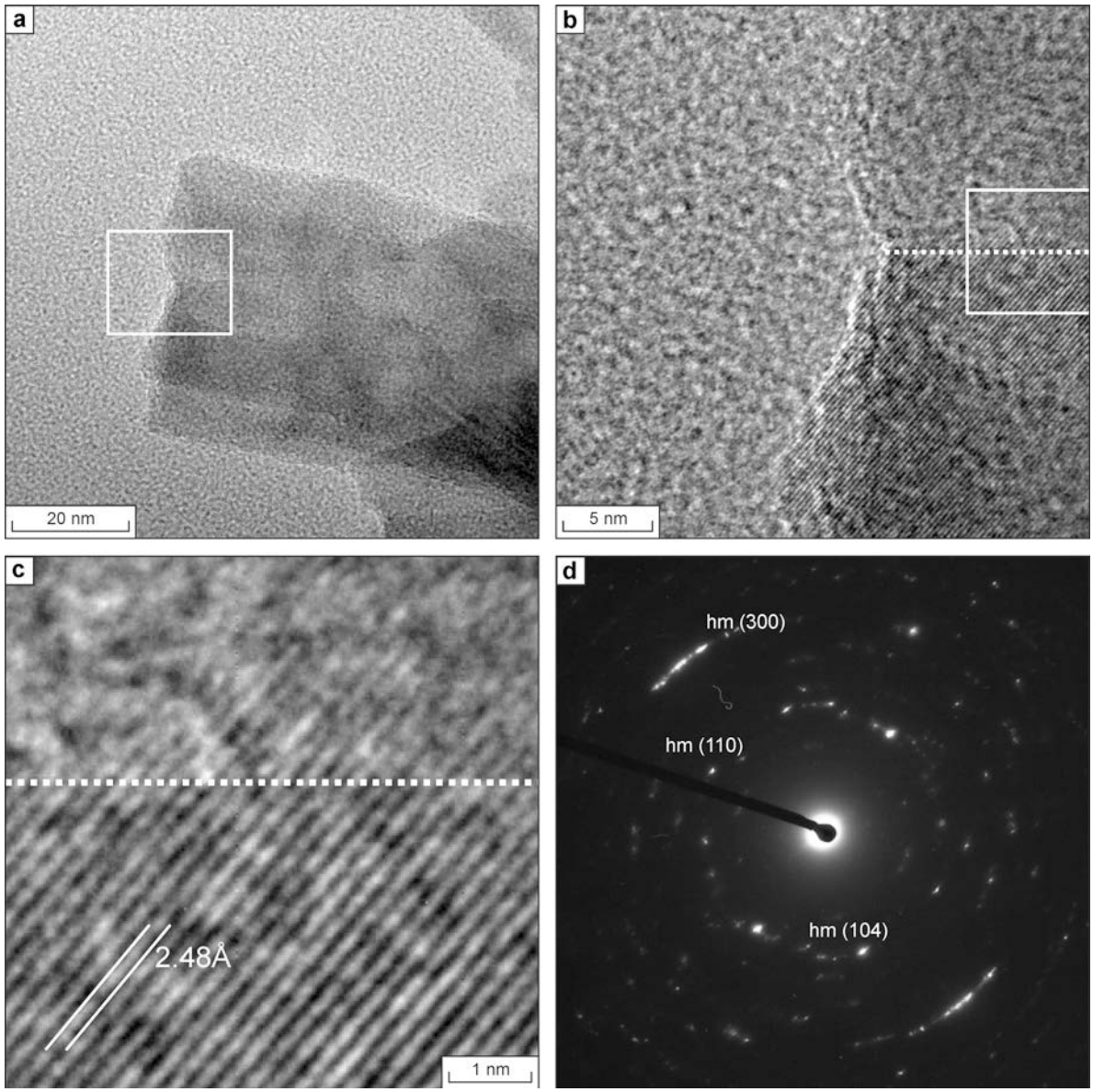

Figure 15. HRTEM image of Weda Bay goethite heated at 800ºC (*i.e.* hematite). (a) The end of a raft consisting of near-parallel, former goethite crystals. (b) Enlargement of (a) showing continuation of hematite lattice fringes across a former boundary (dotted line) between two former goethite crystals. (c) Enlargement of (b) showing that the hematite lattice fringes extend across the former boundary (dotted line) indicating that former goethite crystals have coalesced to form a larger hematite crystal. The 2.48 Å periodicity in the image corresponds to the associated 110 reflection of hematite (2.51 Å) shown in the SAED pattern. Arcing of the hematite (300) reflection (d) indicates that hematite crystals within the compound particle are not arranged in exact parallel alignment.

not all in parallel orientation. The lattice fringes of hematite formed at 800ºC are more extensive than for lower heating temperatures (*i.e.* 340−400ºC), reflecting the increased extent of structural order in hematite particles (Figure 15). Rounded crystals of hematite also occur in goethites heated to high temperatures (Figure 14) and are more abundant for the Ravensthorpe and Kalgoorlie samples. According to Pomiès *et al*. (1999) and Löffler and Mader (2006), spherical crystals become more prevalent with increasing heating temperature (up to 1000ºC) until all the hematite crystals are spherical in shape.

CONCLUSIONS

The results from the TEM investigations, XRD analysis, and thermal analysis of five goethites from oxide-type lateritic Ni ores which were heated to various

https://doi.org/10.1346/CCMN.2009.0570608 Published online by Cambridge University Press

temperatures (220–800ºC) to produce OH-hematite and hematite lead to the following conclusions: (1) Ni substitution into the goethites is quite variable (~0.84–2.08 wt.% Ni). (2) All goethite crystals are acicular in shape and are mostly organized into rafts. (3) The goethites dehydroxylated at different temperatures (262–285ºC). (4) Hematites formed from dehydroxylation of goethite at low temperatures (300–400ºC) are disordered, with much structural or included water. They have small crystal sizes and large surface areas. Hematite formed at higher heating temperatures (600–800ºC), however, contained no water and is better ordered structurally. The needles coalesce and form larger crystals, and the surface area decreases.

The results may contribute to the development of more efficient procedures for the extraction of Ni from lateritic nickel ores. The rate of dissolution of goethite in sulfuric acid (used in 'heap leaching and pressure' leach facilities) is enhanced by increasing the surface area and microporosity of the Fe oxide crystals (Landers and Gilkes, 2007). Therefore, the rate of dissolution of the goethites in sulfuric acid investigated in this paper would be maximized for shock heating temperature between 340 and 400ºC (*i.e.* OH-hematite), where surface area and structural disorder are greatest.

ACKNOWLEDGMENTS

The authors acknowledge the facilities and scientific and technical assistance of the Australian Microscopy & Microanalysis Research Facility at the Centre for Microscopy, Characterisation & Analysis, The University of Western Australia. This facility is funded by The University and State and Commonwealth Governments. Travis Noughton, of the Visual Resources Unit at CSIRO, is thanked for final production of the figures. Thanks to Bruno Lanson, Vidal Barrón, and an anonymous reviewer for their constructive comments which helped improve this article.

REFERENCES

Anand, R.R. and Gilkes, R.J. (1987) The association of maghemite and corundum in Darling Range laterites, Western Australia. *Australian Journal of Soil Research*, **35**, 303–311.

Alvarez, M., Rueda, E.H., and Sileo, E.E. (2007) Simultaneous incorporation of Mn and Al in the goethite structure, *Geochimica et Cosmochimica Acta*, **71**, 1009–1020.

Barrón, V., Gálvez, N., Hochella, M.F., and Torrent, J. (1997) Epitaxial overgrowth of goethite on hematite synthesized in phosphate media: A scanning force and transmission electron microscopy study. *American Mineralogist*, **82**, 1091–1100.

Bernstein, L.R. and Waychunas, G.A. (1987) Germanium crystal chemistry in hematite and goethite from Apex Mine, Utah, and some data on germanium in aqueous solution and in stottite. *Geochimica et Cosmochimica Acta*, **51**, 623–630.

Brown, G. (1980) Associated minerals. Pp. 361–410 in: *Crystal Structures of Clay Minerals and their X-ray Identification* (G.W. Brindley and G.Brown, editors). Monograph **5**, Mineralogical Society, London.

Brunauer, S., Emmett, P.H., and Teller, E. (1938) Adsorption of gases in multimolecular layers. *Journal of the American Chemical Society*, **60**, 309–319.

Carvalho-e-Silva, M.L., Ramos, A.Y., Tolentino, H.C.N., Enweiler, J., Netto, S.M. and Alves, M.C.M. (2003) Incorporation of Ni into natural goethite: An investigation by X-ray absorption spectroscopy. *American Mineralogist*, **88**, 876–882.

Cornell, R.M., Mann, S., and Skarnoulis, A.J. (1983) A high resolution electron microscopy examination of domain boundaries in synthetic goethite. *Journal of the Chemical Society, Faraday Transactions*, **79**, 267–2684.

Cornell, R.M. and Schwertmann, U. (2003) *The Iron Oxides: Structure, Properties, Reactions, Occurrences and Uses*. Wiley-VCH, Weinheim, Germany.

de Faria, D.L.A. and Lopes, F.N. (2007) Heated goethite and natural hematite: Can Raman spectroscopy be used to differentiate them? *Vibrational Spectroscopy*, **45**, 117–121.

Francombe, M.H. and Rooksby, H.P. (1959) Structure transformations affected by the dehydration of diaspore, goethite and delta ferric oxide. *Clay Minerals Bulletin* **4**, 1–14.

Frost, R.L., Kloprogge, J.T., Russell, S.C., and Szetu, J. (1999) Dehydroxylation and the vibrational spectroscopy of aluminum (oxo)hydroxides using infrared emission spectroscopy. Part III: diaspore. *Applied Spectroscopy*, **53**, 829–835.

Frost, R.L., Ding, Z., and Ruan, H.D. (2003) Thermal analysis of goethite, relevance to Australian indigenous art. *Journal of Thermal Analysis and Calorimetry*, **71**, 783–797.

Gerth, J. (1990) Unit-cell dimensions of pure and trace metal-associated goethites. *Geochimica et Cosmochimica Acta*, **54**, 363–371

Golightly, J.P. (1981) Nickeliferous laterite deposits. *Economic Geology*, 75th Anniversary Volume, 710–735.

Gualtieri, A.F. and Venturelli, P. (1999) In situ study of the goethite-hematite phase transformation by real time synchrotron powder diffraction. *American Mineralogist*, **84**, 895–904.

JCPDS (1988) Mineral Powder Diffraction File, Data Book International 635 Center for Diffraction Data, Joint Committee on Powder Diffraction Standards, 636, JCPDS, Pennsylvania, USA.

Klug, H.P. and Alexander, L.E. (1974) *X-ray Diffraction Procedures for Polycrystalline and Amorphous Materials*. John Wiley & Sons, New York.

Landers, M. and Gilkes, R.J. (2007) Dehydroxylation and dissolution of nickeliferous goethite in New Caledonian lateritic Ni ore. *Applied Clay Science*, **35**, 162–172.

Landers, M., Gilkes, R.J., and Wells, M. (2008) Dissolution kinetics of dehydroxylated nickeliferous goethite from limonitic lateritic nickel ore. *Applied Clay Science*, **42**, 615–624.

Löffler, L. and Mader, W. (2006) Anisotropic X-ray peak broadening and twin formation in hematite derived from natural and synthetic goethite. *Journal of the European Ceramic Society*, **26**, 131–139.

Lim-Nunez, R. (1985) Synthesis and acid dissolution of metal substituted goethites and hematites. MSc Thesis, Faculty of Natural and Agricultural Sciences, University of Western Australia.

Lima-de-Faria, J. (1963) Dehydration of goethite and diaspore. *Zeitschrift fur Kristallographie*, **119**, 176–203.

Mackenzie, R.C. and Berggren, G. (1970) Oxides and oxyhydroxides of higher valency elements. Pp. 272–302 in: *Differential Thermal Analysis* (R.C. Mackenzie, editor). Academic Press, London.

Manceau, A., Schlegel, M.L., Musso, M.., Sole, V.A., Gauthier, C., Petit, P.E., and Trolard, F. (2000) Crystal chemistry of trace elements in natural and synthetic goethite. *Geochimica et Cosmochimica Acta*, **64**, 3643–3661.

https://doi.org/10.1346/CCMN.2009.0570608 Published online by Cambridge University Press

Perrier, N., Gilkes, R.J., and Colin, F. (2006) Heating iron rich soils increases the dissolution rate of metals. *Clays and Clay Minerals*, **54**, 165–175.

Pomiès, M.P., Menu, M., and Vignaud, C. (1999) TEM observations of goethite dehydration: Application to archaeological samples. *Journal of the European Ceramic Society*, **19**, 1605–1614.

Pozas, R., Rojas, C.T., Ocana, M., and Serna, C.J. (2004) The nature of Co in synthetic Co-substituted goethites. *Clays and Clay Minerals*, **52**, 760–766.

Rooksby, H.P. (1961) Oxides and hydroxides of aluminium and iron. Pp. 354–392 in: *The X-ray Identification and Crystal Structures of Clay Minerals* (G. Brown, editor). Mineralogical Society, London.

Ruan, H.D. and Gilkes, R.J. (1995) Dehydroxylation of aluminous goethite: Unit cell dimensions, crystal size and surface area. *Clays and Clay Minerals*, **43**, 196–211.

Ruan, H.D., Frost, R.L., Kloprogge, J.T., and Duong, L. (2002) Infrared spectroscopy of goethite dehydroxylation. II. Effect of aluminium substitution on the behaviour of hydroxyl units. *Spectrochimica Acta Part A*, **58**, 479–491.

Rupp, B. (1988) XLAT – a microcomputer program for the refinement of cell constants, *Scripta Metallurgica*, **22**, 69–92.

Schulze, D.G. and Schwertmann, U. (1984) The influence of aluminium on iron oxides, X. Properties of Al-substituted goethites. *Clay Minerals*, **19**, 521–539.

Schwertmann, U., Gasser, U., and Sticher, H. (1989) Chromium-for-iron substitution in synthetic goethites. *Geochimica et Cosmochimica Acta*, **53**, 1293–1297.

Schwertmann, U. and Latham, U. (1986) Properties of iron oxides in some New Caledonian Oxisols. *Geoderma*, **39**, 105–123.

Schwertmann, U. and Pfab, G. (1996) Structural vanadium and chromium in lateritic iron oxides: Genetic implications. *Geochimica et Cosmochimica Acta*, **60**, 4279–4283.

Stiers, W. and Schwertmann, U. (1985) Evidence for manganese substitution in synthetic goethite. *Geochimica et Cosmochimica Acta*, **49**, 1909–1911.

Singh, B. and Gilkes, R.J. (1992a) Properties and distribution of iron oxides and their association with minor elements in the soils of south-western Australia. *Journal of Soil Science*, **43**, 77–98.

Singh, B. and Gilkes, R.J. (1992b) XPAS: An interactive computer program for analysis of powder X-ray diffraction patterns. *Powder Diffraction*, **7**, 6–10.

Torrent, J., Schwertmann, U., and Barrón, V. (1992) Fast and slow phosphate sorption by goethite-rich natural materials. *Clays and Clay Minerals*, **40**, 14–21.

Watari, F., Van Landuyt, J., Delavignette, P., and Amelinckx, S. (1979) Electron microscopic study of dehydration transformations: I. Twin formation and mosaic structure in hematite derived from goethite. *Journal of Solid State Chemistry*, **29**, 137–150.

Watari, F., Van Landuyt, J., Delavignette, P., Amelinekx, S., and Igata, N. (1982) X-ray peak broadening as a result of twin formation in some oxides derived by dehydration. *Physica Status Solidi* (A), **73**, 215–244.

Wells, M.A., Fitzpatrick, R.W., and Gilkes, R.J. (2006) Thermal and mineral properties of Al, Cr, Mn, Ni and Ti-substituted goethite. *Clays and Clay Minerals*, **54**, 176–194.

Wolska, E. (1988) Relationship between the existence of hydroxyl ions in the anionic sublattice of hematite and its infrared and X-ray characteristics. *Solid State Ionics*, **28–30**, 1349–1351.

Wolska, E. and Schwertmann, U. (1989) Nonstoichiometric structures during dehydroxylation of goethite. *Zeitschrift für Kristallographie*, **189**, 223–237.

(*Received 22 October 2008; revised 24 July 2009; Ms. 220; A.E. B.Lanson*)

https://doi.org/10.1346/CCMN.2009.0570608 Published online by Cambridge University Press